Available online at www.sciencedirect.com
SCIENCE DIRECT®
International Journal of Solids and Structures 42 (2005) 2465–2488
INTERNATIONAL JOURNAL OF SOLIDS and STRUCTURES
www.elsevier.com/locate/ijsolstr

Vibration suppression of FGM shells using embedded magnetostrictive layers

S.C. Pradhan *

Department of Aerospace Engineering, Indian Institute of Technology, Kharagpur 721302, India

Received 30 September 2004

Abstract

Analytical solutions of functionally graded material (FGM) shells with embedded magnetostrictive layers are presented in this study. These magnetostrictive layers are used for the vibration suppression of the functionally graded shells. The first-order shear deformation shell theory (FSDT) is employed to study the vibration suppression characteristics. The exact solution for the FGM shell with simply supported boundary conditions is based on the Navier solution procedure. Negative velocity feedback control is used. The parametric effect of the location of the magnetostrictive layers, material properties, and control parameters on the suppression effect are investigated in detail. It is found that (i) the shortest vibration suppression time is achieved by placing the actuating layers farthest from the neutral axis, (ii) the use of thinner smart material layers leads to better vibration attenuation characteristics, and, (iii) the vibration suppression time is longer for a smaller value of the feedback control coefficient.

Keywords: FGM shell; Vibration suppression; Magnetostrictive layers

1. Introduction

A number of materials have been used in sensor/actuator applications. Piezoelectric materials, magnetostrictive materials, shape memory alloys, and electro-rheological fluids have all been integrated with structures to make smart structures. Among these materials piezoelectric, electrostrictive and magnetostrictive materials have the capability to serve as both sensors and actuators. Piezoelectric materials exhibit a

* Corresponding author. Tel.: +91 03222 281750; fax: +91 03222 282422.
E-mail address: scp@aero.iitkgp.ernet.in

0020-7683/$ - see front matter © 2004 Elsevier Ltd. All rights reserved.
doi:10.1016/j.ijsolstr.2004.09.049

Nomenclature

$\mathscr{A}_{31}$, $\mathscr{A}_{32}$, $\mathscr{B}_{31}$, $\mathscr{B}_{32}$ magnetostrictive coefficients integrated over the shell thickness
$\mathscr{B}_{\mathrm{n}}$ normalized $\mathscr{B}_{31}$
α, β positive real number
α_1, α_2 surface metrics
ε_1, ε_2, ε_4, ε_5, ε_6 total strains
ε_1^0, ε_2^0, ε_4^0, ε_5^0, ε_6^0 strains from classical shell theory
ξ_1, ξ_2, ζ orthogonal curvilinear co-ordinates
κ_1, κ_2, κ_6 FSDT strain correction factors
λ eigenvalue
λ_0 arbitrary constant
ϕ_1, ϕ_2 rotational displacements
v_1, v_2 Poisson's ratios of material 1 and material 2
v_{fgm} Poisson's ratio of FGM material 1 and material 2
v_{m} Poisson's ratio of magnetostrictive material
$\rho^{(k)}$ density of kth layer
ρ_{m} density of magnetostrictive material
σ_1, σ_2, σ_4, σ_5, σ_6 stress components
ω_{d} damping frequency
a length of the shell
b breadth of the shell
b_{c} coil width
$c(t)$ control gain
$\mathrm{d}A_1$, $\mathrm{d}A_2$ elementary areas across the thickness of the shell
$\mathrm{d}s$ square of the distance on the middle surface
$\mathrm{d}S$ square of the distance
$e_{31}^{(k)}$, $e_{32}^{(k)}$, $e_{36}^{(k)}$ magnetostrictive material properties of kth layer
g_1, g_2 tangents to ξ_1, ξ_2
h thickness of the shell
k_{c} magnetostrictive coil constant
m, m_1, m_2, n positive integers
n_{c} number of coil turns
nm number of constituent materials in the FGM
q uniformly distributed load in the transverse direction
r position vector on the middle surface
r_{c} coil radius
t_{n} normalized value of t_{s}
t_{s} suppression time ratio
u_1, u_2, u_3 displacements at the middle surface
$\bar{u}_1$, $\bar{u}_2$, $\bar{u}_3$ displacements along ξ_1, ξ_2, ζ
z thickness co-ordinate
$[]^0$ contribution due to classical shell theory
$[]^{\mathrm{M}}$ contribution due to magnetostrictive layer
A_{ij}, B_{ij}, D_{ij} stiffness coefficients of FGM material
C_0 constant depends on R_1 and R_2

E_1, E_2	Young's modulus of material 1 and material 2
E_{fgm}	Young's modulus of FGM material
E_{m}	Young's modulus of magnetostrictive material
G_{fgm}	shear modulus of FGM material
H	magnetic field intensity
I	coil current intensity
I_1, I_2, I_3	moment of inertia
K_{S}	shear correction factor
L_1, L_2, L_3	Lame' coefficients
M_1, M_2, M_6	moments applied on the edges of the shell
M^{M}	moments due to the magnetostrictive layer
N	number of layers assumed for computation
N_1, N_2, N_6	forces applied on the edges of the shell
N^{M}	forces due to the magnetostrictive layer
P_{-1}, P_1, P_2, P_3	FGM material constants
P_{fgm}	material property of the FGM material
P_i	material properties of the constituents of the FGM material
Q_1, Q_2	shear forces applied on the edges of the shell
$Q_{ij}^{(k)}$	stiffness coefficients of kth layer
R	position vector of arbitrary point
R_1, R_2	principal radii of curvature of the middle surface of the shell
R_n	positive real number
S_{ij}, C_{ij}, M_{ij}	coefficients of stiffness, damping and mass matrices
$\overline{S}_{ij}$	coefficients of solution matrix
T	temperature
V_{c}	volume fraction of ceramic material
$V_{\text{f}i}$	volume fraction of the constituents of FGM material
V_{m}	volume fraction of metal material
$W_{\max}$	maximum amplitude in transverse direction
Z_{m}	transverse location of magnetostrictive layer in the FGM shell

linear relationship between the electric field and strains for low field values (up to 100 V/mm). This relationship is nonlinear for large fields, and the material exhibits hysteresis (Uchino, 1986). Further, piezoelectric materials show dielectric aging and hence lack reproducibility of strains, i.e. a drift from zero state of strain is observed under cyclic electric field applications (Cross and Jang, 1988).

Crawley and Luis (1987) demonstrated the feasibility of using piezoelectric actuators for free vibration reduction of a cantilever beam. Baz et al. (1990) investigated vibration control using shape memory alloy and carried out their characterization. Choi et al. (1990) demonstrated the vibration reduction effects of electro-rheological fluid actuators in a composite beam. An ideal actuator, for distributed embedded application, should have high energy density, negligible weight, and point excitation with a wide frequency bandwidth. Terfenol-D, a magnetostrictive material, has the characteristics of being able to produce strains up to 2000 and an energy density as high as $0.0025\,\text{J}\,\text{m}^{-3}$ in response to a magnetic field. Goodfriend and Shoop (1992) reviewed the material properties of Terfenol-D with regard to its use in vibration isolation. Anjanappa and Bi (1994) investigated the feasibility of using embedded magnetostrictive mini actuators for smart structure applications, such as vibration suppression of beams. Bryant et al. (1993) presented experimental results of a magnetostrictive Terfenol-D rod used in dual capacity of passive structural support

element and an active vibration control actuator. Krishna Murty et al. (1997) proposed magnetostrictive actuators that take advantage of ease with which the actuators can be embedded, and the use of remotely excitation capability of magnetostrictive particle as new actuators for smart structures. This work is limited to flexible beam theory.

Friedmann et al. (2001) used magnetostrictive material Terfenol-D in high speed helicopter rotors and studied the vibration reduction characteristics. Vibration and shape control of flexible structures is achieved with the help of actuators and a control law. Response of FGM shells are also studied by He et al. (2002), Woo and Meguid (2001), Pradhan et al. (2000) and Loy et al. (1999). Many modern techniques have been developed in recent years to meet the challenge of designing controllers that suit the function under required conditions. There have been a number of studies on vibration control of flexible structures using magnetostrictive materials (Anjanappa and Bi, 1994; Bryant et al., 1993; Krishna Murty et al., 1997; Giurgiutiu et al., 2001; Pradhan et al., 2001). Although there have been important research efforts devoted to characterizing the properties of Terfelon-D material, fundamental information about variation in elasto-magnetic material properties in a functionally graded shell is not available.

In the present study vibration control of functionally graded shells are studied using the first-order shear deformation theory. Exact solutions are developed for simply supported doubly curved functionally graded shells with magnetostrictive layers. This closed form solution exists for FGM shells where the coefficients A_{16}, A_{26}, B_{16}, B_{26}, D_{16}, D_{26}, A_{45} are equal to zero. A simple negative velocity feedback control is used to actively control the dynamic response of the structure through a closed loop control. Numerical results of vibration suppression effect for various locations of the magnetostrictive layers, material properties, and control parameters are presented.

2. Theoretical formulation

2.1. Kinematic description

Fig. 1a contains a differential element of a doubly curved shell element with constant curvatures along coordinate directions ξ_1 and ξ_2 (Reddy, 1984a). ξ_1, ξ_2 and ζ denote the orthogonal curvilinear coordinates such that ξ_1 and ξ_2 curves are the lines of curvature on the middle surface ($\zeta = 0$). Thus, for the doubly curved shell panel considered here, the lines of the principal curvature coincide with the coordinate lines. The values of the principal radii of curvature of the middle surface are denoted by R_1 and R_2. The position vector of a point $(\xi_1, \xi_2, 0)$ on the middle surface is denoted by $\mathbf{r}$, and the position of an arbitrary point (ξ_1, ξ_2, ζ) is denoted by $\mathbf{R}$ (see Fig. 1b). The square of the distance ds between points $(\xi_1, \xi_2, 0)$ and $(\xi_1 + \mathrm{d}\xi_1, \xi_2 + \mathrm{d}\xi_2, 0)$ is determined by

$$(\mathrm{d}s)^2 = \mathrm{d}\mathbf{r} \cdot \mathrm{d}\mathbf{r} = \alpha_1^2 (\mathrm{d}\xi_1)^2 + \alpha_2^2 (\mathrm{d}\xi_2)^2 \tag{1}$$

in which $\mathrm{d}\mathbf{r} = \mathbf{g}_1 \mathrm{d}\xi_1 + \mathbf{g}_2 \mathrm{d}\xi_2$, the vectors $\mathbf{g}_1$ and $\mathbf{g}_2$ ($\mathbf{g}_i = \frac{\partial \mathbf{r}}{\partial \xi_i}$) are tangents to the ξ_1 and ξ_2 coordinate lines and α_1 and α_2 are the surface metrics

$$\alpha_1^2 = \mathbf{g}_1 \cdot \mathbf{g}_1, \quad \alpha_2^2 = \mathbf{g}_2 \cdot \mathbf{g}_2 \tag{2}$$

The square of the distance dS between (ξ_1, ξ_2, ζ) and $(\xi_1 + \mathrm{d}\xi_1, \xi_2 + \mathrm{d}\xi_2, \zeta + \mathrm{d}\zeta)$ is given by

$$(\mathrm{d}S)^2 = \mathrm{d}\mathbf{R} \cdot \mathrm{d}\mathbf{R} = L_1^2 (\mathrm{d}\xi_1)^2 + L_2^2 (\mathrm{d}\xi_2)^2 + L_3^2 (\mathrm{d}\zeta)^2 \tag{3}$$

in which $\mathrm{d}\mathbf{R} = (\frac{\partial \mathbf{R}}{\partial \xi_1})\mathrm{d}\xi_1 + (\frac{\partial \mathbf{R}}{\partial \xi_2})\mathrm{d}\xi_2 + (\frac{\partial \mathbf{R}}{\partial \zeta})\mathrm{d}\zeta$ and L_1, L_2, and L_3 are the Lame' coefficients (Reddy, 1984a)

$$L_1 = \alpha_1 \left(1 + \frac{\zeta}{R_1}\right), \quad L_2 = \alpha_2 \left(1 + \frac{\zeta}{R_2}\right), \quad L_3 = 1 \tag{4}$$

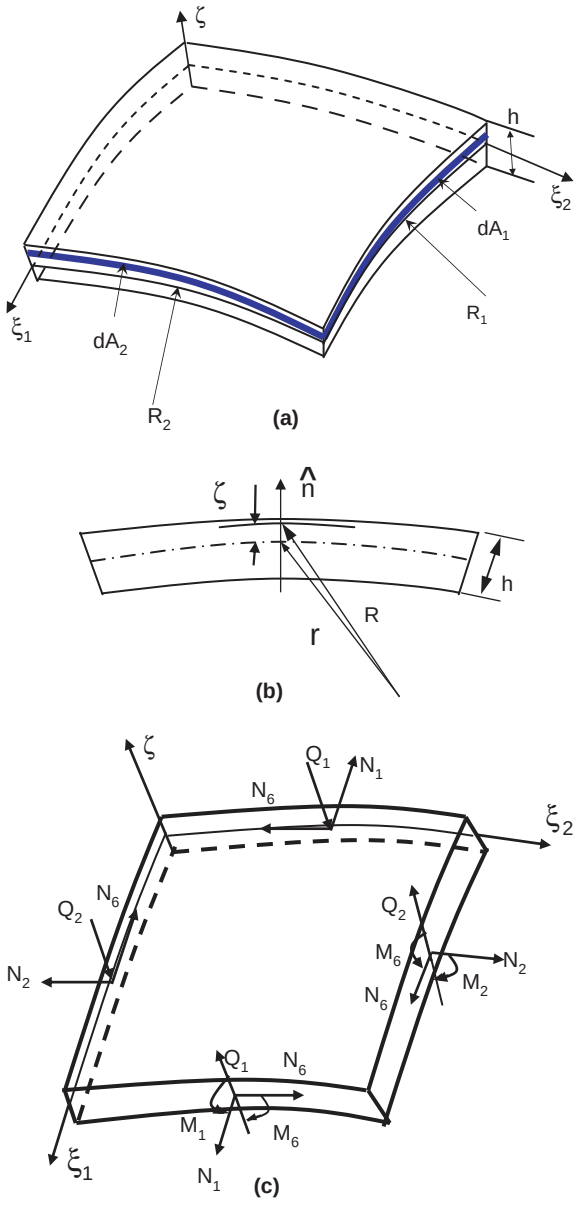

Fig. 1. Geometry and stress resultants of doubly curved shell.

From Fig. 1a, the elements of area of the cross sections are

$$\begin{aligned} \mathrm{d}A_1 &= L_1\,\mathrm{d}\xi_1\,\mathrm{d}\zeta = \alpha_1\left(1+\frac{\zeta}{R_1}\right)\mathrm{d}\xi_1\,\mathrm{d}\zeta \\ \mathrm{d}A_2 &= L_2\,\mathrm{d}\xi_2\,\mathrm{d}\zeta = \alpha_2\left(1+\frac{\zeta}{R_2}\right)\mathrm{d}\xi_2\,\mathrm{d}\zeta \end{aligned} \tag{5}$$

Next, we introduce the stress resultants acting on a shell element. For example, N_1 denotes the tensile force measured per unit length along a ξ_2 coordinate line on a cross section perpendicular to a ξ_1 coordinate line (see Fig. 1c). The total tensile force on the differential element in the ξ_1 direction is $N_1\alpha_2 \mathrm{d}\xi_2$. This force is equal to the integral $\sigma_1 \mathrm{d}A_2$ over the thickness

$$N_1\alpha_2 \mathrm{d}\xi_2 = \int_{-h/2}^{h/2} \sigma_1 \mathrm{d}A_2 \tag{6}$$

where h the total thickness of the shell ($\zeta = -h/2$ and $\zeta = h/2$ denotes the bottom and top surface of the shell). Using Eq. (5) we can write

$$N_1 = \int_{-h/2}^{h/2} \sigma_1 \left(1 + \frac{\zeta}{R_2}\right) \mathrm{d}\zeta \tag{7}$$

Similarly, the remaining stress resultants per unit length can be defined. The complete set of expression for forces and moments are written as (Reddy, 1984a)

$$\begin{Bmatrix} N_1 \\ N_2 \\ N_6 \\ N_6 \\ Q_1 \\ Q_2 \\ M_1 \\ M_2 \\ M_6 \\ M_6 \end{Bmatrix} = \int_{-h/2}^{h/2} \begin{Bmatrix} \sigma_1\left(1+\frac{\zeta}{R_2}\right) \\ \sigma_2\left(1+\frac{\zeta}{R_1}\right) \\ \sigma_6\left(1+\frac{\zeta}{R_2}\right) \\ \sigma_6\left(1+\frac{\zeta}{R_1}\right) \\ \sigma_5\left(1+\frac{\zeta}{R_2}\right) \\ \sigma_4\left(1+\frac{\zeta}{R_1}\right) \\ \zeta\sigma_1\left(1+\frac{\zeta}{R_2}\right) \\ \zeta\sigma_2\left(1+\frac{\zeta}{R_1}\right) \\ \zeta\sigma_6\left(1+\frac{\zeta}{R_2}\right) \\ \zeta\sigma_6\left(1+\frac{\zeta}{R_1}\right) \end{Bmatrix} \mathrm{d}\zeta \tag{8}$$

For shallow shells, one can neglect ζ/R_1 and ζ/R_2 terms as in a plate theory. The shear forces Q_i are often corrected by introducing shear correction factor K_S:

$$\begin{Bmatrix} Q_1 \\ Q_2 \end{Bmatrix} = K_S \int_{-h/2}^{h/2} \begin{Bmatrix} \sigma_5\left(1+\frac{\zeta}{R_2}\right) \\ \sigma_4\left(1+\frac{\zeta}{R_1}\right) \end{Bmatrix} \mathrm{d}\zeta \tag{9}$$

2.2. Displacement field

We assume the following form of the displacement field that is consistent with the assumptions of a moderately thick shell or Sanders shell theory (Reddy, 1984b).

$$\begin{aligned} \bar{u}_1(\xi_1,\xi_2,\zeta,t) &= \frac{L_1}{\alpha_1} u_1(\xi_1,\xi_2,t) + \zeta\phi_1(\xi_1,\xi_2,t) \\ \bar{u}_2(\xi_1,\xi_2,\zeta,t) &= \frac{L_2}{\alpha_2} u_2(\xi_1,\xi_2,t) + \zeta\phi_2(\xi_1,\xi_2,t) \\ \bar{u}_3(\xi_1,\xi_2,\zeta,t) &= u_3(\xi_1,\xi_2,t) \end{aligned} \tag{10}$$

in which $(\bar{u}_1, \bar{u}_2, \bar{u}_3)$ are the displacements of a point (ξ_1, ξ_2, ζ) along the (ξ_1, ξ_2, ζ) coordinates; and $(u_1, u_2, u_3) =$ displacements of a point $(\xi_1, \xi_2, 0)$ on the mid surface of the shell. Substituting Eq. (10) into strain–displacement relations for the first-order shear deformation theory, one obtains

$$\begin{Bmatrix} \varepsilon_1 \\ \varepsilon_2 \\ \varepsilon_4 \\ \varepsilon_5 \\ \varepsilon_6 \end{Bmatrix} = \begin{Bmatrix} \varepsilon_1^0 \\ \varepsilon_2^0 \\ \varepsilon_4^0 \\ \varepsilon_5^0 \\ \varepsilon_6^0 \end{Bmatrix} + \zeta \begin{Bmatrix} \kappa_1 \\ \kappa_2 \\ 0 \\ 0 \\ \kappa_6 \end{Bmatrix} \tag{11}$$

where

$$\begin{Bmatrix} \varepsilon_1^0 \\ \varepsilon_2^0 \\ \varepsilon_4^0 \\ \varepsilon_5^0 \\ \varepsilon_6^0 \end{Bmatrix} = \begin{Bmatrix} \frac{1}{\alpha_1}\frac{\partial u_1}{\partial \xi_1} + \frac{1}{R_1}u_3 \\ \frac{1}{\alpha_2}\frac{\partial u_2}{\partial \xi_2} + \frac{1}{R_2}u_3 \\ \frac{1}{\alpha_2}\frac{\partial u_3}{\partial \xi_2} + \phi_2 - \frac{1}{R_2}u_2 \\ \frac{1}{\alpha_1}\frac{\partial u_3}{\partial \xi_1} + \phi_1 - \frac{1}{R_1}u_1 \\ \frac{1}{\alpha_1}\frac{\partial u_2}{\partial \xi_1} + \frac{1}{\alpha_2}\frac{\partial u_1}{\partial \xi_2} \end{Bmatrix} \tag{12}$$

$$\begin{aligned} \kappa_1 &= \frac{1}{\alpha_1}\frac{\partial \phi_1}{\partial \xi_1}, \quad \kappa_2 = \frac{1}{\alpha_2}\frac{\partial \phi_2}{\partial \xi_2} \\ \kappa_6 &= \frac{1}{\alpha_1}\frac{\partial \phi_2}{\partial \xi_1} + \frac{1}{\alpha_2}\frac{\partial \phi_1}{\partial \xi_2} + \frac{1}{2}\left(\frac{1}{R_2} - \frac{1}{R_1}\right)\left(\frac{1}{\alpha_1}\frac{\partial u_2}{\partial \xi_1} - \frac{1}{\alpha_2}\frac{\partial u_1}{\partial \xi_2}\right) \end{aligned} \tag{13}$$

and (ϕ_1, ϕ_2) are rotations of a transverse normal line about the ξ_2 and ξ_1 coordinate axes, respectively.

$$\phi_1 = -\frac{\partial u_3}{\partial \xi_1}, \quad \phi_2 = -\frac{\partial u_3}{\partial \xi_2} \tag{14}$$

2.3. Equations of motion

The displacement field (10) can be used to derive the governing equations of the first-order shear deformation theory of shells. By means of Hamilton's principle (or the dynamic version of the principle of virtual displacements), one can obtain the following governing equations of motion in terms of the displacements and stress resultants in the Cartesian coordinate system $(x_1, x_2, x_3 = \zeta)$ (assuming that $N_{12} = N_{21} = N_6$ and $M_{12} = M_{21} = M_6$):

$$\begin{aligned} &\frac{\partial N_1}{\partial x_1} + \frac{\partial}{\partial x_2}(N_6 + C_0 M_6) + \frac{Q_1}{R_1} = \left(I_1 + 2\frac{I_2}{R_1}\right)\frac{\partial^2 u_1}{\partial t^2} + \left(I_1 + \frac{I_3}{R_1}\right)\frac{\partial^2 \phi_1}{\partial t^2} \\ &\frac{\partial}{\partial x_1}(N_6 - C_0 M_6) + \frac{\partial N_2}{\partial x_2} + \frac{Q_2}{R_2} = \left(I_1 + 2\frac{I_2}{R_2}\right)\frac{\partial^2 u_2}{\partial t^2} + \left(I_1 + \frac{I_3}{R_2}\right)\frac{\partial^2 \phi_2}{\partial t^2} \\ &\frac{\partial Q_1}{\partial x_1} + \frac{\partial Q_2}{\partial x_2} - \left(\frac{N_1}{R_1} + \frac{N_2}{R_2}\right) + q = I_1\frac{\partial^2 u_3}{\partial t^2} \\ &\frac{\partial M_1}{\partial x_1} + \frac{\partial M_6}{\partial x_2} - Q_1 = I_2\frac{\partial^2 \phi_1}{\partial t^2} + \left(I_1 + \frac{I_3}{R_1}\right)\frac{\partial^2 u_1}{\partial t^2} \\ &\frac{\partial M_6}{\partial x_1} + \frac{\partial M_2}{\partial x_2} - Q_2 = I_2\frac{\partial^2 \phi_2}{\partial t^2} + \left(I_1 + \frac{I_3}{R_2}\right)\frac{\partial^2 u_2}{\partial t^2} \end{aligned} \tag{15}$$

where

$$C_0 = \frac{1}{2}\left(\frac{1}{R_1} - \frac{1}{R_2}\right), \quad \frac{1}{\partial x_i} = \frac{1}{\alpha_i}\frac{1}{\partial \xi_i} \quad (i = 1, 2), \quad I_i = \sum_{k=1}^{N} \int_{\zeta_k}^{\zeta_{k+1}} \rho^{(k)} (\zeta)^{i-1} \, \mathrm{d}\zeta \quad (i = 1, 2, 3) \tag{16}$$

and $\rho^{(k)}$ is the density of the kth layer. N is the number of layers assumed for computation.

2.4. Constitutive relations

Suppose that the shell is composed of N functionally graded layers. The stress–strain relations of the kth layer, whether structural layer or actuating/sensing layer, in the shell coordinate system are given as

$$\begin{Bmatrix} \sigma_1 \\ \sigma_2 \\ \sigma_4 \\ \sigma_5 \\ \sigma_6 \end{Bmatrix}^{(k)} = \begin{bmatrix} Q_{11} & Q_{12} & 0 & 0 & 0 \\ Q_{12} & Q_{22} & 0 & 0 & 0 \\ 0 & 0 & Q_{44} & 0 & 0 \\ 0 & 0 & 0 & Q_{55} & 0 \\ 0 & 0 & 0 & 0 & Q_{66} \end{bmatrix}^{(k)} \begin{Bmatrix} \varepsilon_1 \\ \varepsilon_2 \\ \varepsilon_4 \\ \varepsilon_5 \\ \varepsilon_6 \end{Bmatrix} - \zeta \begin{Bmatrix} e_{31} \\ e_{32} \\ 0 \\ 0 \\ e_{36} \end{Bmatrix}^{(k)} H \tag{17}$$

where $Q_{ij}^{(k)}$ are the stiffnesses of kth layer and

$$\begin{aligned} &Q_{11} = \frac{E_{\mathrm{fgm}}}{1 - \nu_{\mathrm{fgm}}^2}, \quad Q_{12} = \frac{\nu_{\mathrm{fgm}} E_{\mathrm{fgm}}}{1 - \nu_{\mathrm{fgm}}^2}, \quad Q_{22} = Q_{11} \\ &Q_{44} = Q_{55} = Q_{66} = G_{\mathrm{fgm}} \end{aligned} \tag{18}$$

The superscript k on Q_{ij} as well as on the engineering constants E_{fgm}, ν_{fgm} and so on are omitted for brevity. In Eq. (17), H denotes the intensity of the magnetic field. H is applied normal to the thickness of the shell. e_{ij} are the magnetostrictive material coefficients.

2.5. Feedback control

A velocity feedback control is used in the present study. In the velocity feed back control, the magnetic field intensity H is expressed in terms of coil current $I(\xi_1, \xi_2, t)$

$$H(\xi_1, \xi_2, t) = k_{\mathrm{c}} I(\xi_1, \xi_2, t) \tag{19}$$

Current I is related to the transverse velocity by

$$I(\xi_1, \xi_2, t) = c(t) \frac{\partial u_3(\xi_1, \xi_2, t)}{\partial t} \tag{20}$$

where k_{c} is the magnetic coil constant and is related to the number of coil turns n_{c}, coil width b_{c}, and coil radius r_{c}

$$k_{\mathrm{c}} = \frac{n_{\mathrm{c}}}{\sqrt{b_{\mathrm{c}}^2 + 4r_{\mathrm{c}}^2}} \tag{21}$$

The parameter $c(t)$ is known as the control gain.

2.6. Functionally graded material

FGM are basically particles in matrix composite materials, which are made by mixing two or more different materials. Most of the FGM are being used in high temperature environment and their material

properties are temperature dependent. A typical material property P_i can be expressed as a function of the environment temperature $T(K)$

$$P_i = P_0(P_{-1}T^{-1} + 1 + P_1T + P_2T^2 + P_3T^3) \tag{22}$$

where, P_0, P_{-1}, P_1, P_2 and P_3 are temperature coefficients and are unique to the constituent materials. The material properties P_{fgm} of FGM are controlled by volume fractions $V_{\text{f}i}$ and individual material properties P_i of the constituent materials.

$$P_{\text{fgm}} = \sum_{i=1}^{nm} P_i V_{\text{f}i} \tag{23}$$

In the present case two different materials are particle mixed to form the FGM material. A schematic of FGM shell with magnetostrictive layers is shown in Fig. 2a and b. In Fig. 2a it is shown that two layers of magnetostrictive materials are placed symmetrically away from the neutral plane of the FGM shell. A zoomed view of section AA of Fig. 2a is shown in Fig. 2b. Assuming there are no defects like voids and foreign particles in the FGM material, sum of the volume fractions of all the constituent materials is unity.

$$\sum_{i=1}^{nm} V_{\text{f}i} = 1 \tag{24}$$

For example, metal and ceramic materials ($nm = 2$) are mixed to form the FGM shell. Average volume fraction of the metal and ceramic materials are calculated by simple integration of the distribution over

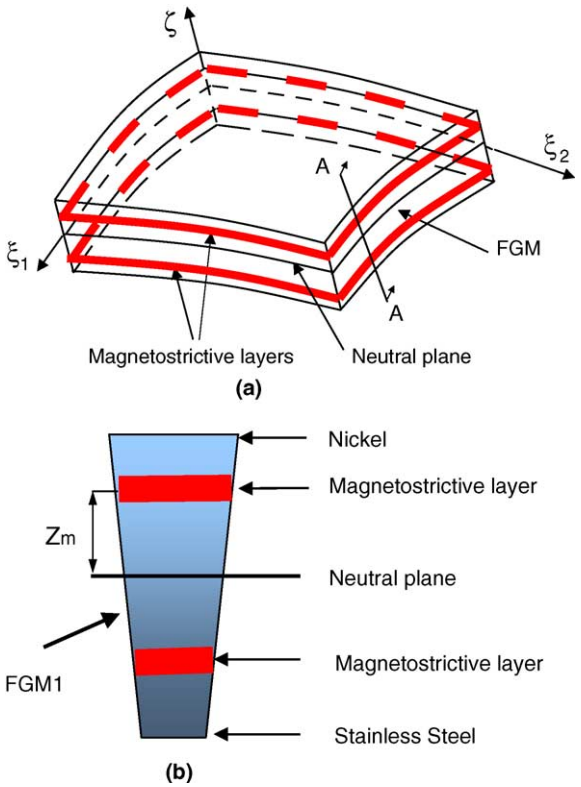

Fig. 2. Functionally graded shell with embedded magnetostrictive layers.

a domain. Different problems of interest have different expressions of volume fractions. For bending problems of plates and shells the volume fractions of metal (V_m) and ceramic (V_c) materials are defined as

$$V_m = \left(\frac{h-2z}{2h}\right)^{R_n}$$
$$V_c = 1 - V_m \tag{25}$$

where z is the thickness co-ordinate ($-h/2 \leqslant z \leqslant h/2$) and h represents the shell thickness. R_n is the power law exponent ($0 \leqslant R_n \leqslant \infty$). Here volume fraction of the metal material (V_m) varies from 100% to 0% as z

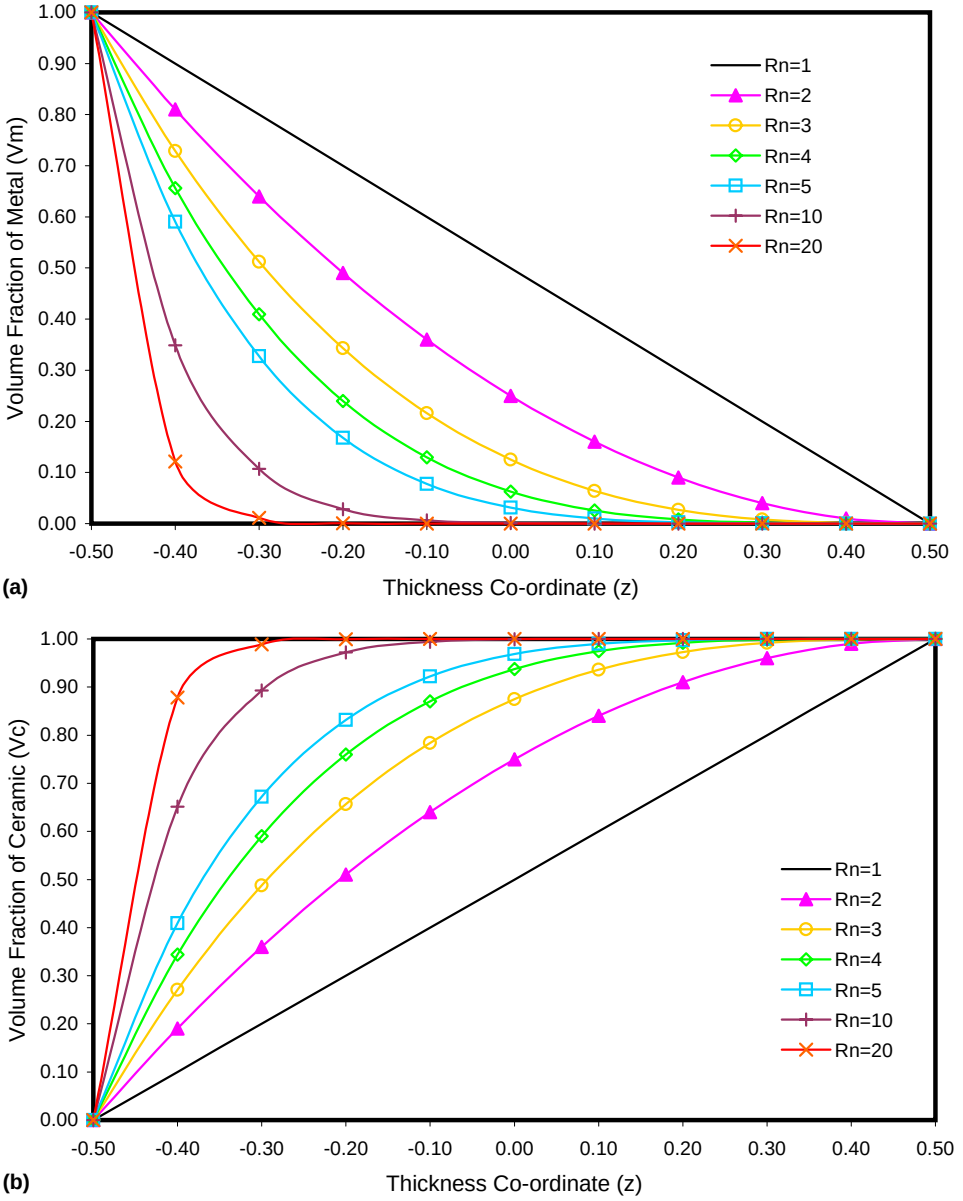

Fig. 3. Volume fractions of metal and ceramic materials in the FGM shell.

Table 1
Material properties of FGM constituent materials

	Stainless Steel		Nickel		Aluminum Oxide	
Density ($kg\,m^{-3}$)	7900		8909		3970	
Coefficient	E ($N\,m^{-2}$)	v	E ($N\,m^{-2}$)	v	E ($N\,m^{-2}$)	v
P_0	201.04E09	0.3262	244.27E09	0.2882	349.55E09	0.260
P_{-1}	0	0	0	0	0	0
P_1	3.079E−04	−2.002E−04	−1.371E−03	1.133E−04	−3.853E−04	0
P_2	−6.534E−07	3.797E−07	1.214E−06	0	4.027E−07	0
P_3	0	0	−3.681E−10	0	−1.673E−10	0

varies from $-h/2$ to $h/2$. Similarly volume fraction of the ceramic material (V_c) varies from 0% to 100% as z varies from $-h/2$ to $h/2$. For various R_n values the average volume fractions of metal (V_m) and ceramic (V_c) materials are depicted in Fig. 3a and b, respectively. The Young's modulus and Poisson's ratio of a FGM shell made up of two different materials are expressed as

$$E_{fgm} = (E_2 - E_1)\left(\frac{2z+h}{2h}\right)^{R_n} + E_1 \tag{26}$$

$$v_{fgm} = (v_2 - v_1)\left(\frac{2z+h}{2h}\right)^{R_n} + v_1 \tag{27}$$

E_1, E_2 and E_{fgm} are the Young's moduli of the constituent materials and the FGM material, respectively. v_1, v_2 and v_{fgm} are the Poisson's ratios of the constituent materials and the FGM material, respectively. From these equations ((26) and (27)), it is interesting to note that at $z = -h/2$, FGM material properties are same as those of material 1. While at $z = h/2$, FGM material properties are same as those of material 2. Thus, the FGM material properties vary smoothly across thickness, from material 1 at the inner surface to material 2 at the outer surface.

Two different FGM materials are considered for the present study viz. FGM1 and FGM2. FGM1 consists of Stainless Steel and Nickel materials (Fig. 2b). FGM2 consists of Nickel and Aluminum Oxide materials. Material properties of Stainless Steel, Nickel materials and Aluminum Oxide are listed in Table 1. In the present work, we have used the room temperature to calculate the material properties of the FGM shells.

3. Analytical solution

Analytical solutions of the set of equations (15) can be obtained for simply supported functionally graded shell panels. Towards using the Navier type solution, first we write the governing equations in terms of the displacements. Using the constitutive equations, the layer constitutive equations can be expressed as (Reddy, 1984a)

$$\begin{Bmatrix} \{N\} \\ \{M\} \end{Bmatrix} = \begin{bmatrix} [A] & [B] \\ [B] & [D] \end{bmatrix} \begin{Bmatrix} \{\varepsilon^0\} \\ \{\kappa\} \end{Bmatrix} - \begin{Bmatrix} \{N\} \\ \{M\} \end{Bmatrix}^{M} \tag{28}$$

$$\begin{Bmatrix} Q_2 \\ Q_1 \end{Bmatrix} = K_S \begin{bmatrix} A_{44} & A_{45} \\ A_{45} & A_{55} \end{bmatrix} \begin{Bmatrix} \varepsilon_4^0 \\ \varepsilon_5^0 \end{Bmatrix} - \begin{Bmatrix} Q_2^M \\ Q_1^M \end{Bmatrix} \tag{29}$$

where the laminate stiffness coefficients (A_{ij}, B_{ij}, D_{ij}) are defined by

$$\begin{aligned} A_{ij} &= \sum_{k=1}^{N} Q_{ij}^{(k)}(\zeta_{k+1}-\zeta_k), \quad i,j=1,2,6 \\ B_{ij} &= \frac{1}{2}\sum_{k=1}^{N} Q_{ij}^{(k)}(\zeta_{k+1}^2-\zeta_k^2), \quad i,j=1,2,6 \\ D_{ij} &= \frac{1}{3}\sum_{k=1}^{N} Q_{ij}^{(k)}(\zeta_{k+1}^3-\zeta_k^3), \quad i,j=1,2,6 \\ A_{ij} &= \sum_{k=1}^{N} Q_{ij}^{(k)}(\zeta_{k+1}-\zeta_k), \quad i,j=4,5 \end{aligned} \tag{30}$$

and the magnetostrictive stress resultants $\{N^{\mathrm{M}}\}$ and $\{M^{\mathrm{M}}\}$ are defined as

$$\begin{Bmatrix} N_1^{\mathrm{M}} \\ N_2^{\mathrm{M}} \end{Bmatrix} = \sum_{k=m_1,m_2,\ldots}^{N} \int_{\zeta_k}^{\zeta_{k+1}} \begin{Bmatrix} e_{31} \\ e_{32} \end{Bmatrix} H_\zeta \,\mathrm{d}\zeta = ck_{\mathrm{c}} \sum_{k=m_1,m_2,\ldots}^{N} \int_{\zeta_k}^{\zeta_{k+1}} \begin{Bmatrix} e_{31} \\ e_{32} \end{Bmatrix} \frac{\partial u_3}{\partial t}\,\mathrm{d}\zeta \equiv \begin{Bmatrix} \mathscr{A}_{31} \\ \mathscr{A}_{32} \end{Bmatrix} \frac{\partial u_3}{\partial t} \tag{31}$$

$$\begin{Bmatrix} M_1^{\mathrm{M}} \\ M_2^{\mathrm{M}} \end{Bmatrix} = \sum_{k=m_1,m_2,\ldots}^{N} \int_{\zeta_k}^{\zeta_{k+1}} \begin{Bmatrix} e_{31} \\ e_{32} \end{Bmatrix} \zeta H_\zeta \,\mathrm{d}\zeta = ck_{\mathrm{c}} \sum_{k=m_1,m_2,\ldots}^{N} \int_{\zeta_k}^{\zeta_{k+1}} \begin{Bmatrix} e_{31} \\ e_{32} \end{Bmatrix} \frac{\partial u_3}{\partial t}\,\zeta\,\mathrm{d}\zeta \equiv \begin{Bmatrix} \mathscr{B}_{31} \\ \mathscr{B}_{32} \end{Bmatrix} \frac{\partial u_3}{\partial t} \tag{32}$$

where

$$\begin{aligned} \mathscr{A}_{ij} &= ck_{\mathrm{c}} \sum_{k=m_1,m_2,\ldots} e_{ij}^{(k)}(\zeta_{k+1}-\zeta_k), \quad i=3;\ j=1,2 \\ \mathscr{B}_{ij} &= \frac{1}{2}ck_{\mathrm{c}} \sum_{k=m_1,m_2,\ldots} e_{ij}^{(k)}(\zeta_{k+1}^2-\zeta_k^2), \quad i=3;\ j=1,2 \end{aligned} \tag{33}$$

and m_1, m_2,... denote the layer numbers of the magnetostrictive (or any actuating/sensing) layers. The equations of motion (15) can be expressed in terms of displacements $(u_1, u_2, u_3, \phi_1, \phi_2)$ by substituting for the force and moment resultants from Eqs. (28) and (29). For homogeneous laminates, the equations of motion (15) take the following form (Reddy, 1984a)

δu_1:

$$\begin{aligned} &A_{11}\left(\frac{\partial^2 u_1}{\partial x_1^2}+\frac{1}{R_1}\frac{\partial u_3}{\partial x_1}\right)+A_{12}\left(\frac{\partial^2 u_2}{\partial x_1\partial x_2}+\frac{1}{R_2}\frac{\partial u_3}{\partial x_1}\right)+A_{16}\left(\frac{\partial^2 u_2}{\partial x_1^2}+\frac{\partial^2 u_1}{\partial x_1\partial x_2}\right)+B_{11}\frac{\partial^2\phi_1}{\partial x_1^2}+B_{12}\frac{\partial^2\phi_2}{\partial x_1\partial x_2} \\ &+B_{16}\left[\frac{\partial^2\phi_2}{\partial x_1^2}+\frac{\partial^2\phi_1}{\partial x_1\partial x_2}-C_0\left(\frac{\partial^2 u_2}{\partial x_1^2}-\frac{\partial^2 u_1}{\partial x_1\partial x_2}\right)\right]+A_{16}\left(\frac{\partial^2 u_1}{\partial x_1\partial x_2}+\frac{1}{R_1}\frac{\partial u_3}{\partial x_2}\right)+A_{26}\left(\frac{\partial^2 u_2}{\partial x_2^2}+\frac{1}{R_2}\frac{\partial u_3}{\partial x_2}\right) \\ &+A_{66}\left(\frac{\partial^2 u_2}{\partial x_1\partial x_2}+\frac{\partial^2 u_1}{\partial x_2^2}\right)+B_{16}\frac{\partial^2\phi_1}{\partial x_1\partial x_2}+B_{26}\frac{\partial^2\phi_2}{\partial x_2^2}+B_{66}\left[\frac{\partial^2\phi_2}{\partial x_1\partial x_2}+\frac{\partial^2\phi_1}{\partial x_2^2}-C_0\left(\frac{\partial^2 u_2}{\partial x_1\partial x_2}-\frac{\partial^2 u_1}{\partial x_2^2}\right)\right] \\ &-\mathscr{A}_{31}\frac{\partial^2 u_3}{\partial x_1\partial t}+\frac{1}{R_1}\left[K_{\mathrm{S}}A_{44}\left(\phi_1+\frac{\partial u_3}{\partial x_1}-\frac{u_1}{R_1}\right)+K_{\mathrm{S}}A_{45}\left(\phi_2+\frac{\partial u_3}{\partial x_2}-\frac{u_2}{R_2}\right)\right]-\left(I_1+2\frac{I_2}{R_1}\right)\frac{\partial^2 u_1}{\partial t^2} \\ &-\left(I_1+\frac{I_3}{R_1}\right)\frac{\partial^2\phi_1}{\partial t^2} \\ &=0 \end{aligned} \tag{34}$$

δu_2:

$$
\begin{aligned}
&A_{12}\left(\frac{\partial^2 u_1}{\partial x_1 \partial x_2}+\frac{1}{R_1}\frac{\partial u_3}{\partial x_2}\right)+A_{22}\left(\frac{\partial^2 u_2}{\partial x_2^2}+\frac{1}{R_2}\frac{\partial u_3}{\partial x_2}\right)+A_{26}\left(\frac{\partial^2 u_2}{\partial x_1 \partial x_2}+\frac{\partial^2 u_1}{\partial x_2^2}\right)+B_{12}\frac{\partial^2 \phi_1}{\partial x_1 \partial x_2}+B_{22}\frac{\partial^2 \phi_2}{\partial x_2^2}\\
&+B_{26}\left[\frac{\partial^2 \phi_2}{\partial x_1 \partial x_2}+\frac{\partial^2 \phi_1}{\partial x_2^2}-C_0\left(\frac{\partial^2 u_2}{\partial x_1 \partial x_2}-\frac{\partial^2 u_1}{\partial x_2^2}\right)\right]+A_{16}\left(\frac{\partial^2 u_1}{\partial x_1^2}+\frac{1}{R_1}\frac{\partial u_3}{\partial x_1}\right)+A_{26}\left(\frac{\partial^2 u_2}{\partial x_1 \partial x_2}+\frac{1}{R_2}\frac{\partial u_3}{\partial x_1}\right)\\
&+A_{66}\left(\frac{\partial^2 u_2}{\partial x_1^2}+\frac{\partial^2 u_1}{\partial x_1 \partial x_2}\right)+B_{16}\frac{\partial^2 \phi_1}{\partial x_1^2}+B_{26}\frac{\partial^2 \phi_2}{\partial x_1 \partial x_2}+B_{66}\left[\frac{\partial^2 \phi_2}{\partial x_1^2}+\frac{\partial^2 \phi_1}{\partial x_2 \partial x_1}-C_0\left(\frac{\partial^2 u_2}{\partial x_1^2}-\frac{\partial^2 u_1}{\partial x_1 \partial x_2}\right)\right]\\
&-\mathscr{A}_{32}\frac{\partial^2 u_3}{\partial x_2 \partial t}+\frac{1}{R_2}\left[K_S A_{45}\left(\phi_1+\frac{\partial u_3}{\partial x_1}-\frac{u_1}{R_1}\right)+K_S A_{55}\left(\phi_2+\frac{\partial u_3}{\partial x_2}-\frac{u_2}{R_2}\right)\right]-\left(I_1+2\frac{I_1}{R_2}\right)\frac{\partial^2 u_2}{\partial t^2}\\
&-\left(I_1+\frac{I_3}{R_2}\right)\frac{\partial^2 \phi_2}{\partial t^2}\\
&=0
\end{aligned}
\tag{35}
$$

δu_3:

$$
\begin{aligned}
&K_S A_{45}\left(\frac{\partial^2 u_3}{\partial x_1 \partial x_2}+\frac{\partial \phi_2}{\partial x_1}-\frac{\partial u_2}{R_2 \partial x_1}\right)+K_S A_{55}\left(\frac{\partial^2 u_3}{\partial^2 x_1}+\frac{\partial \phi_1}{\partial x_1}-\frac{\partial u_1}{R_1 \partial x_1}\right)+K_S A_{44}\left(\frac{\partial^2 u_3}{\partial^2 x_2}+\frac{\partial \phi_2}{\partial x_2}-\frac{\partial u_2}{R_2 \partial x_2}\right)\\
&+K_S A_{45}\left(\frac{\partial^2 u_3}{\partial x_1 \partial x_2}+\frac{\partial \phi_1}{\partial x_2}-\frac{\partial u_1}{R_1 \partial x_2}\right)-\frac{1}{R_1}\left\{A_{11}\left(\frac{\partial u_1}{\partial x_1}+\frac{u_3}{R_1}\right)+A_{12}\left(\frac{\partial u_2}{\partial x_2}+\frac{u_3}{R_2}\right)+A_{16}\left(\frac{\partial u_2}{\partial x_1}+\frac{\partial u_1}{\partial x_2}\right)\right.\\
&\left.+B_{11}\frac{\partial \phi_1}{\partial x_1}+B_{12}\frac{\partial \phi_2}{\partial x_2}+B_{16}\left[\frac{\partial \phi_2}{\partial x_1}+\frac{\partial \phi_1}{\partial x_2}-C_0\left(\frac{\partial u_2}{\partial x_1}+\frac{\partial u_1}{\partial x_2}\right)\right]-\mathscr{A}_{31}\frac{\partial u_3}{\partial t}\right\}\\
&-\frac{1}{R_2}\left\{A_{12}\left(\frac{\partial u_1}{\partial x_1}+\frac{u_3}{R_1}\right)+A_{22}\left(\frac{\partial u_2}{\partial x_2}+\frac{u_3}{R_2}\right)+A_{26}\left(\frac{\partial u_2}{\partial x_1}-\frac{\partial u_1}{\partial x_2}\right)+B_{12}\frac{\partial \phi_1}{\partial x_1}+B_{22}\frac{\partial \phi_2}{\partial x_1}\right.\\
&\left.+B_{26}\left[\frac{\partial \phi_2}{\partial x_1}+\frac{\partial \phi_1}{\partial x_2}-C_0\left(\frac{\partial u_2}{\partial x_1}-\frac{\partial u_1}{\partial x_2}\right)\right]-\mathscr{A}_{32}\frac{\partial u_3}{\partial t}\right\}+q-I_1\frac{\partial^2 u_3}{\partial t^2}\\
&=0
\end{aligned}
\tag{36}
$$

$\delta \phi_1$:

$$
\begin{aligned}
&B_{11}\left(\frac{\partial^2 u_1}{\partial x_1^2}+\frac{\partial u_3}{R_1 \partial x_1}\right)+B_{12}\left(\frac{\partial^2 u_2}{\partial x_1 \partial x_2}+\frac{\partial u_3}{R_2 \partial x_1}\right)+B_{16}\left(\frac{\partial^2 u_2}{\partial x_1^2}+\frac{\partial^2 u_1}{\partial x_1 \partial x_2}\right)+D_{11}\frac{\partial^2 \phi_1}{\partial x_1^2}+D_{12}\frac{\partial^2 \phi_2}{\partial x_1 \partial x_2}\\
&+D_{16}\left[\frac{\partial^2 \phi_2}{\partial x_1^2}+\frac{\partial^2 \phi_1}{\partial x_1 \partial x_2}-C_0\left(\frac{\partial^2 u_2}{\partial x_1^2}-\frac{\partial^2 u_1}{\partial x_1 \partial x_2}\right)\right]+B_{16}\left(\frac{\partial^2 u_1}{\partial x_1 \partial x_2}+\frac{\partial u_3}{R_1 \partial x_2}\right)+B_{26}\left(\frac{\partial^2 u_2}{\partial x_2^2}+\frac{\partial u_3}{R_2 \partial x_2}\right)\\
&+B_{66}\left(\frac{\partial^2 u_2}{\partial x_1 \partial x_2}+\frac{\partial^2 u_1}{\partial x_2^2}\right)+D_{16}\frac{\partial^2 \phi_1}{\partial x_1 \partial x_2}+D_{26}\frac{\partial^2 \phi_2}{\partial x_2^2}+D_{66}\left[\frac{\partial^2 \phi_2}{\partial x_1 \partial x_2}+\frac{\partial^2 \phi_1}{\partial x_2^2}-C_0\left(\frac{\partial^2 u_2}{\partial x_1 \partial x_2}-\frac{\partial^2 u_1}{\partial x_2^2}\right)\right]\\
&+K_S A_{45}\left(\frac{\partial u_3}{\partial x_2}+\phi_2-\frac{u_2}{R_2}\right)+K_S A_{55}\left(\frac{\partial u_3}{\partial x_1}+\phi_1-\frac{u_1}{R_1}\right)-\mathscr{B}_{31}\frac{\partial^2 u_3}{\partial x_1 \partial t}-I_2\frac{\partial^2 \phi_1}{\partial t^2}-\left(I_1+\frac{I_3}{R_1}\right)\frac{\partial^2 u_1}{\partial t^2}\\
&=0
\end{aligned}
\tag{37}
$$

$\delta\phi_2$:

$$
\begin{aligned}
&B_{16}\left(\frac{\partial^2 u_1}{\partial x_1^2}+\frac{\partial u_3}{R_1\partial x_1}\right)+B_{26}\left(\frac{\partial^2 u_2}{\partial x_1\partial x_2}+\frac{\partial u_3}{R_2\partial x_1}\right)+B_{66}\left(\frac{\partial^2 u_2}{\partial x_1^2}+\frac{\partial^2 u_1}{\partial x_1\partial x_2}\right)+D_{16}\frac{\partial^2\phi_1}{\partial x_1^2}+D_{26}\frac{\partial^2\phi_2}{\partial x_1\partial x_2}\\
&+D_{66}\left[\frac{\partial^2\phi_2}{\partial x_1^2}+\frac{\partial^2\phi_1}{\partial x_1\partial x_2}+\frac{1}{2}\left(\frac{1}{R_2}-\frac{1}{R_1}\right)\left(\frac{\partial^2 u_2}{\partial x_1^2}-\frac{\partial^2 u_1}{\partial x_1\partial x_2}\right)\right]+B_{12}\left(\frac{\partial^2 u_1}{\partial x_1\partial x_2}+\frac{\partial u_3}{R_1\partial x_2}\right)\\
&+B_{22}\left(\frac{\partial^2 u_2}{\partial x_2^2}+\frac{\partial u_3}{R_2\partial x_2}\right)+B_{66}\left(\frac{\partial^2 u_2}{\partial x_1\partial x_2}+\frac{\partial^2 u_1}{\partial x_2^2}\right)+D_{12}\frac{\partial^2\phi_1}{\partial x_1\partial x_2}+D_{22}\frac{\partial^2\phi_2}{\partial x_2^2}\\
&+D_{26}\left[\frac{\partial^2\phi_2}{\partial x_1\partial x_2}+\frac{\partial^2\phi_1}{\partial x_2^2}+\frac{1}{2}\left(\frac{1}{R_2}-\frac{1}{R_1}\right)\left(\frac{\partial^2 u_2}{\partial x_1\partial x_2}-\frac{\partial^2 u_1}{\partial x_2^2}\right)\right]+K_S A_{44}\left(\frac{\partial u_3}{\partial x_2}+\phi_2-\frac{u_2}{R_2}\right)\\
&+K_S A_{45}\left(\frac{\partial u_3}{\partial x_1}+\phi_1-\frac{u_1}{R_1}\right)-\mathscr{B}_{32}\frac{\partial^2 u_3}{\partial x_2\partial t}-I_2\frac{\partial^2\phi_2}{\partial t^2}-\left(I_1+\frac{I_3}{R_2}\right)\frac{\partial^2 u_2}{\partial t^2}\\
&=0
\end{aligned}
\tag{38}
$$

Eqs. (34)–(38) describe five second-order, nonlinear, partial differential equations in terms of the five generalized displacements. The simply supported boundary conditions for the first-order shear deformation shell theory (FSDT) are

$$
\begin{aligned}
&u_1(x_1,0,t)=0,\quad u_1(x_1,b,t)=0,\quad u_2(0,x_2,t)=0,\quad u_2(a,x_2,t)=0\\
&\phi_1(x_1,0,t)=0,\quad \phi_1(x_1,b,t)=0,\quad \phi_2(0,x_2,t)=0,\quad \phi_2(a,x_2,t)=0\\
&u_3(x_1,0,t)=0,\quad u_3(x_2,b,t)=0,\quad u_3(0,x_2,t)=0,\quad u_3(a,x_2,t)=0
\end{aligned}
\tag{39}
$$

The boundary conditions in Eq. (39) are satisfied by the following expansions (Reddy, 1984a)

$$
\begin{aligned}
q(x_1,x_2,t)&=\sum_{m,n=1}^{\infty}Q_{mn}(t)\sin\alpha x_1\sin\beta x_2\\
u_1(x_1,x_2,t)&=\sum_{m,n=1}^{\infty}U_{mn}(t)\cos\alpha x_1\sin\beta x_2\\
u_2(x_1,x_2,t)&=\sum_{m,n=1}^{\infty}V_{mn}(t)\sin\alpha x_1\cos\beta x_2\\
u_3(x_1,x_2,t)&=\sum_{m,n=1}^{\infty}W_{mn}(t)\sin\alpha x_1\sin\beta x_2\\
\phi_1(x_1,x_2,t)&=\sum_{m,n=1}^{\infty}X_{mn}(t)\cos\alpha x_1\sin\beta x_2\\
\phi_2(x_1,x_2,t)&=\sum_{m,n=1}^{\infty}Y_{mn}(t)\sin\alpha x_1\cos\beta x_2
\end{aligned}
\tag{40}
$$

where $\alpha=m\pi/a$ and $\beta=n\pi/b$.

Substituting for Eqs. (39) and (40) into Eqs. (34)–(38) yields the equations

$$\begin{bmatrix} S_{11} & S_{12} & S_{13} & S_{14} & S_{15} \\ S_{21} & S_{22} & S_{23} & S_{24} & S_{25} \\ S_{31} & S_{32} & S_{33} & S_{34} & S_{35} \\ S_{41} & S_{42} & S_{43} & S_{44} & S_{45} \\ S_{51} & S_{52} & S_{53} & S_{54} & S_{55} \end{bmatrix} \begin{Bmatrix} U_{mn} \\ V_{mn} \\ W_{mn} \\ X_{mn} \\ Y_{mn} \end{Bmatrix} + \begin{bmatrix} 0 & 0 & C_{13} & 0 & 0 \\ 0 & 0 & C_{23} & 0 & 0 \\ 0 & 0 & C_{33} & 0 & 0 \\ 0 & 0 & C_{43} & 0 & 0 \\ 0 & 0 & C_{53} & 0 & 0 \end{bmatrix} \begin{Bmatrix} \dot{U}_{mn} \\ \dot{V}_{mn} \\ \dot{W}_{mn} \\ \dot{X}_{mn} \\ \dot{Y}_{mn} \end{Bmatrix}$$
$$+ \begin{bmatrix} M_{11} & 0 & 0 & M_{14} & 0 \\ 0 & M_{22} & 0 & 0 & M_{25} \\ 0 & 0 & M_{33} & 0 & 0 \\ M_{41} & 0 & 0 & M_{44} & 0 \\ 0 & M_{52} & 0 & 0 & M_{55} \end{bmatrix} \begin{Bmatrix} \ddot{U}_{mn} \\ \ddot{V}_{mn} \\ \ddot{W}_{mn} \\ \ddot{X}_{mn} \\ \ddot{Y}_{mn} \end{Bmatrix} = \begin{Bmatrix} 0 \\ 0 \\ Q_{mn} \\ 0 \\ 0 \end{Bmatrix} \tag{41}$$

where S_{ij}, C_{ij} and M_{ij} $(i,j = 1,2,\ldots,5)$ are defined in Appendix A.

Here the magnetostrictive coefficients $\mathscr{A}_{31}$, $\mathscr{A}_{32}$, $\mathscr{B}_{31}$ and $\mathscr{B}_{32}$ are defined in Eq. (33). For vibration control, we assume the uniformly distributed transverse load $q = 0$ and seek solution of the ordinary differential equations in Eq. (41) in the form

$$U_{mn}(t) = U_0 e^{\lambda t}, \quad V_{mn}(t) = V_0 e^{\lambda t}, \quad W_{mn}(t) = W_0 e^{\lambda t}, \quad X_{mn}(t) = X_0 e^{\lambda t}, \quad Y_{mn}(t) = Y_0 e^{\lambda t} \tag{42}$$

Substituting Eq. (42) into Eq. (41), for a nontrivial solution we obtain the result

$$\begin{vmatrix} \overline{S}_{11} & \overline{S}_{12} & \overline{S}_{13} & \overline{S}_{14} & \overline{S}_{15} \\ \overline{S}_{21} & \overline{S}_{22} & \overline{S}_{23} & \overline{S}_{24} & \overline{S}_{25} \\ \overline{S}_{31} & \overline{S}_{32} & \overline{S}_{33} & \overline{S}_{34} & \overline{S}_{35} \\ \overline{S}_{41} & \overline{S}_{42} & \overline{S}_{43} & \overline{S}_{44} & \overline{S}_{45} \\ \overline{S}_{51} & \overline{S}_{52} & \overline{S}_{53} & \overline{S}_{54} & \overline{S}_{55} \end{vmatrix} = 0 \tag{43}$$

where

$$\overline{S}_{ij} = S_{ij} + \lambda C_{ij} + \lambda^2 M_{ij} \tag{44}$$

for $i,j = 1,2,3,4,5$. This equation gives five sets of eigenvalues. The lowest one corresponds to the transverse motion. The eigenvalue can be written as $\lambda = -\lambda_0 + i\omega_d$, so that the damped motion is given by

$$u_3(x_1,x_2,t) = \frac{1}{\omega_d} e^{-\lambda_0 t} \sin \omega_d t \sin \frac{n\pi x_1}{a} \sin \frac{n\pi x_2}{b} \tag{45}$$

In arriving at the last solution, the following initial conditions are used:

$$\begin{aligned} &u_1(x_1,x_2,0) = 0, \quad \dot{u}_1(x_1,x_2,0) = 0, \quad u_2(x_1,x_2,0) = 0, \\ &\dot{u}_2(x_1,x_2,0) = 0, \quad u_3(x_1,x_2,0) = 0, \quad \dot{u}_3(x_1,x_2,0) = 1, \\ &\phi_1(x_1,x_2,0) = 0, \quad \dot{\phi}_1(x_1,x_2,0) = 0, \quad \phi_2(x_1,x_2,0) = 0, \\ &\dot{\phi}_2(x_1,x_2,0) = 0 \end{aligned} \tag{46}$$

4. Results and discussion

In the present work a theoretical analysis of a functionally graded material (FGM) shell, consisting of layers of magnetostrictive material. The magnetostrictive material is assumed to impart vibration control

through a velocity dependent feedback law that controls the current to the magnetic coils energizing the magnetostrictive material. First-order shear deformation theory (FSDT) is used in the derivation. Numerical simulation results are presented. Effect of various parameters on the vibration suppression time is studied. These parameters are (a) location of magnetostrictive layer from the neutral plane, (b) thickness of magnetostrictive layer, (c) higher modes of vibration, (d) material properties of magnetostrictive material and (e) material properties of FGM material.

The FGM shell is considered to be of $1\,\mathrm{m} \times 1\,\mathrm{m}$ dimension. Two different types of FGM shells (FGM1 and FGM2) are considered for the present study. FGM1 is made up of Stainless Steel and Nickel. FGM2 is made up of Nickel and Aluminum Oxide. For most of the present work FGM1 is employed. In the present work if it is not mentioned FGM2 means it is FGM1 shell. The material properties of constituent materials, Stainless Steel, Nickel and Aluminum Oxide of the FGM shells are listed in Table 1. Two layers of magnetostrictive materials are placed symmetrically away from the neutral plane of the FGM shell. These layers are shown in Fig. 2a. A zoomed view of section AA of Fig. 2a is shown in Fig. 2b. Magnetostrictive material properties are considered to be

$$E_{\mathrm{m}} = 26.5\,\mathrm{GPa}, \quad \nu_{\mathrm{m}} = 0.0, \quad \rho_{\mathrm{m}} = 9250\,\mathrm{kg\,m^{-3}}, \quad c(t) r_{\mathrm{c}} = 10^4 \tag{47}$$

The numerical values of various materials and structural constants based on different locations of magnetostrictive layers and FGM material properties are listed in Tables 2 and 3.

Table 2
Various coefficients of FGM1 (Stainless Steel–Nickel) shell

Z_{m}/m	D_{11}/N m (10^6)	D_{12}/N m (10^5)	D_{66}/N m (10^5)	A_{44}/N m^{-1} (10^{10})	I_1/kg m^{-1} (10^2)	I_3/kg m (10^{-2})	$-\mathscr{A}_{31}$ (10^2)	$-\mathscr{B}_{31}$ (10^4)	$\mathscr{B}_{\mathrm{n}}$
0.0095	0.124	0.376	0.434	0.311	0.849	0.287	0.926	0.879	1.000
0.0085	0.132	0.401	0.460	0.311	0.849	0.286	0.926	0.787	0.895
0.0075	0.139	0.423	0.484	0.311	0.849	0.285	0.926	0.694	0.790
0.0065	0.145	0.442	0.505	0.311	0.849	0.284	0.926	0.601	0.684
0.0055	0.150	0.459	0.523	0.311	0.849	0.283	0.926	0.509	0.579
0.0045	0.155	0.473	0.538	0.311	0.849	0.282	0.926	0.416	0.473
0.0035	0.158	0.484	0.550	0.311	0.849	0.281	0.926	0.324	0.369
0.0025	0.161	0.492	0.558	0.311	0.849	0.280	0.926	0.231	0.263
0.0015	0.162	0.498	0.564	0.311	0.849	0.280	0.926	0.138	0.157
0.0005	0.163	0.501	0.567	0.311	0.849	0.280	0.926	0.046	0.052

Table 3
Various coefficients of FGM2 (Nickel–Aluminum Oxide) shell

Z_{m}/m	D_{11}/N m (10^6)	D_{12}/N m (10^5)	D_{66}/N m (10^5)	A_{44}/N m^{-1} (10^{10})	I_1/kg m^{-1} (10^2)	I_3/kg m (10^{-2})	$-\mathscr{A}_{31}$ (10^2)	$-\mathscr{B}_{31}$ (10^4)	$\mathscr{B}_{\mathrm{n}}$
0.0095	0.161	0.436	0.586	0.424	0.672	0.240	0.926	0.879	1.000
0.0085	0.171	0.465	0.625	0.424	0.672	0.235	0.926	0.787	0.895
0.0075	0.181	0.491	0.658	0.424	0.672	0.230	0.926	0.695	0.791
0.0065	0.189	0.514	0.688	0.424	0.672	0.226	0.926	0.602	0.685
0.0055	0.196	0.533	0.713	0.424	0.672	0.223	0.926	0.509	0.579
0.0045	0.202	0.549	0.735	0.424	0.672	0.220	0.926	0.417	0.474
0.0035	0.206	0.563	0.752	0.424	0.672	0.218	0.926	0.324	0.369
0.0025	0.210	0.573	0.764	0.424	0.672	0.216	0.926	0.231	0.263
0.0015	0.213	0.579	0.773	0.424	0.672	0.215	0.926	0.139	0.158
0.0005	0.213	0.582	0.777	0.424	0.672	0.215	0.926	0.046	0.052

In this study, the vibration suppression time (t_s) is defined as the time required to reduce the uncontrolled vibration amplitude to one-tenth of its initial amplitude. In the present numerical simulations the suppression time, thickness of the magnetostrictive layer are denoted by t_s and h_m, respectively. In Fig. 2b, Z_m represents the distance between the location of the magnetostrictive layer and the neutral plane.

4.1. Effect of magnetostrictive layer location

Effect of location of magnetostrictive layers on the vibration suppression is studied. Fig. 2a and b show the location of magnetostrictive layers in the FGM shells. Transverse deflection versus time for Z_m of 9.5 mm, 7.5 mm, 5.5 mm and 3.5 mm are plotted in Fig. 4a–d, respectively. For Z_m equals to 9.5 mm Fig. 4a shows shortest suppression time (t_s) of 0.22 s and for Z_m equals to 3.5 mm Fig. 4d shows longest suppression time (t_s) of 0.59 s. From Fig. 4a–d, shortest suppression time is observed when the magnetostrictive layers are placed farther away from the neutral plane. Similarly, from Fig. 4a–d one can observe that, longest suppression time occurs when the magnetostrictive layer is located closest to the neutral plane of the shell.

Influence of the position of the magnetostrictive layers in the thickness direction from the neutral plane of the shell on the damping of the vibration response are listed in Tables 4–7. In Tables 4–7, the value of λ_0 [see Eq. (36)] increases when the magnetostrictive layer is located farther away from the neutral axis,

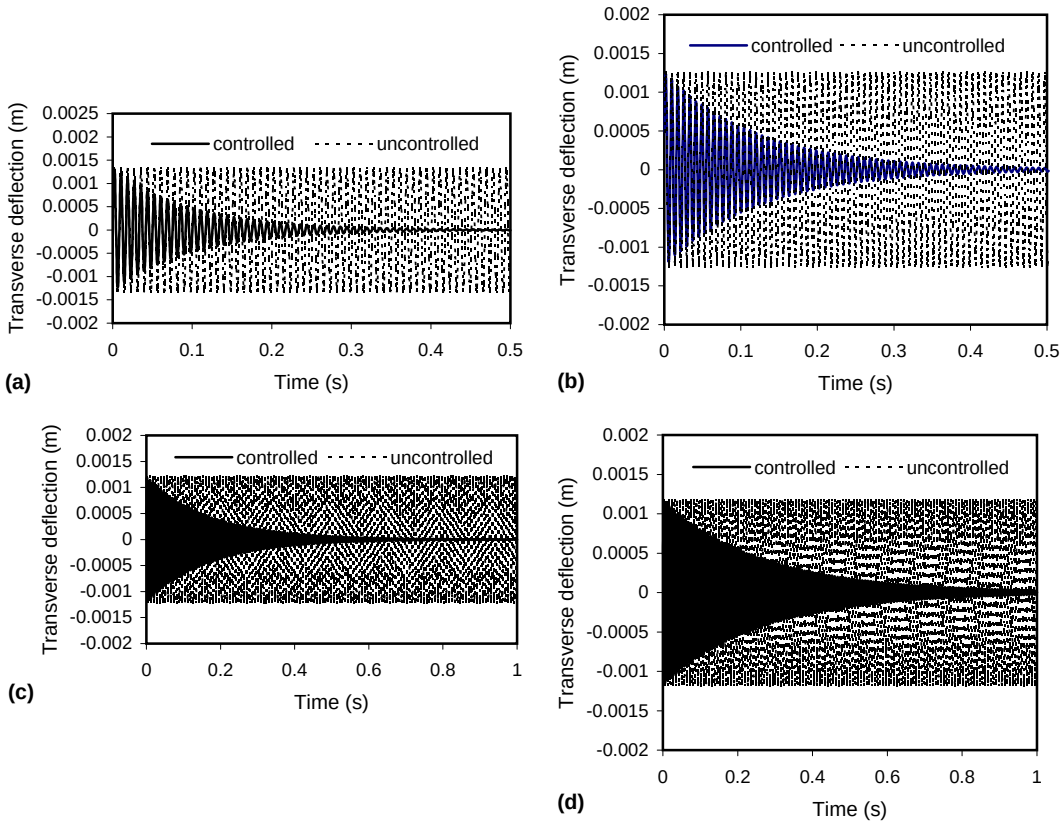

Fig. 4. Comparison of uncontrolled (---) and controlled (—) motion at the midpoint of the FGM1 shell for various locations of magnetostrictive layers, (a) $Z_m = 9.5$ mm, (b) $Z_m = 7.5$ mm, (c) $Z_m = 5.5$ mm and (d) $Z_m = 3.5$ mm.

Table 4
Suppression time ratio for various locations of magnetostrictive layers in FGM1 laminates $h_m = 1$ mm

Z_m (m)	$-\lambda_0$	$\pm\omega_d$	W_{max} (mm)	t_s (s)	t_n
0.0095	10.212	752.04	1.329	0.228	0.053
0.0085	9.136	776.53	1.287	0.237	0.055
0.0075	8.061	799.46	1.230	0.277	0.064
0.0065	6.986	813.75	1.209	0.311	0.072
0.0055	5.911	829.02	1.187	0.371	0.086
0.0045	4.836	845.02	1.163	0.448	0.104
0.0035	3.761	851.32	1.155	0.592	0.137
0.0025	2.686	858.55	1.146	0.825	0.191
0.0015	1.612	858.64	1.449	1.378	0.319
0.0005	0.537	859.11	1.153	4.311	1.000

Table 5
Suppression time ratio for various locations of magnetostrictive layers in FGM1 laminates $h_m = 2$ mm

Z_m (m)	$-\lambda_0$	$\pm\omega_d$	W_{max} (mm)	t_s (s)	t_n
0.0095	20.335	1517.54	0.644	0.117	0.057
0.0085	18.191	1546.49	0.634	0.129	0.063
0.0075	16.049	1588.18	0.619	0.144	0.070
0.0065	13.906	1631.74	0.603	0.165	0.081
0.0055	11.766	1639.97	0.601	0.192	0.093
0.0045	9.625	1686.26	0.583	0.230	0.112
0.0035	7.486	1709.38	0.575	0.295	0.143
0.0025	5.346	1724.01	0.570	0.402	0.195
0.0015	3.208	1712.36	0.576	0.675	0.328
0.0005	1.069	1720.58	0.575	2.058	1.000

Table 6
Suppression time ratio for various locations of magnetostrictive layers in FGM1 laminates $h_m = 3$ mm

Z_m (m)	$-\lambda_0$	$\pm\omega_d$	W_{max} (mm)	t_s (s)	t_n
0.0095	30.285	2254.90	0.398	0.080	0.057
0.0085	27.086	2327.05	0.389	0.088	0.062
0.0075	23.891	2380.03	0.385	0.095	0.067
0.0065	20.699	2432.79	0.381	0.105	0.074
0.0055	17.509	2479.42	0.378	0.131	0.093
0.0045	14.323	2507.17	0.376	0.149	0.105
0.0035	11.138	2545.09	0.373	0.186	0.132
0.0025	7.954	2557.24	0.375	0.273	0.193
0.0015	4.773	2572.12	0.379	0.471	0.333
0.0005	1.591	2580.25	0.383	1.413	1.000

indicating faster vibration suppression. This is due to the larger bending moment created by actuating force in the magnetostrictive layers. Further, it is observed that the damping parameter $\mathscr{B}_{31}$ and associated normalized value of $\mathscr{B}_n$ increases as the magnetostrictive layers are moved away from the neutral plane. These damping parameters are listed in Tables 2 and 3. These results agree qualitatively with the results presented in Pradhan et al. (2001) and He et al. (2002).

Table 7
Suppression time ratio for two different control gains and various locations of magnetostrictive layers in FGM1 laminates $h_m = 5$ mm

Z_m (m)	$C(t)r_c = 10^4$					$C(t)r_c = 10^3$				
	$-\lambda_0$	$\pm\omega_d$	W_{max} (mm)	t_s (s)	t_n	$-\lambda_0$	$\pm\omega_d$	W_{max} (mm)	t_s (s)	t_n
0.0475	49.367	3707.84	0.252	0.049	0.051	4.936	3708.17	0.262	0.495	0.051
0.0425	44.121	3826.31	0.240	0.057	0.059	4.412	3826.56	0.253	0.570	0.059
0.0375	38.893	3922.18	0.235	0.064	0.067	3.889	3922.37	0.252	0.645	0.067
0.0325	33.680	4004.38	0.230	0.068	0.071	3.368	4004.52	0.245	0.680	0.071
0.0275	28.477	4072.82	0.222	0.086	0.090	2.847	4072.91	0.241	0.861	0.090
0.0225	23.285	4133.77	0.211	0.101	0.105	2.328	4133.84	0.236	1.011	0.105
0.0175	18.102	4180.22	0.205	0.129	0.135	1.810	4180.25	0.219	1.292	0.135
0.0125	12.926	4211.51	0.203	0.181	0.189	1.292	4211.53	0.217	1.813	0.189
0.0075	7.753	4234.36	0.201	0.112	0.325	0.775	4234.37	0.229	3.122	0.325
0.0025	2.584	4248.35	0.220	0.959	1.000	0.258	4248.35	0.233	9.594	1.000

4.2. Effect of thickness of magnetostrictive layers

Vibration response of FGM1 shell for various thicknesses of the magnetostrictive layers (h_m) are studied. Magnetostrictive damping coefficients and natural frequencies for various thicknesses of magnetostrictive layers are listed in Tables 4–7. These damping coefficients and natural frequencies refer to the first mode of vibration. Vibration suppression time for h_m equals to 1 mm, 2 mm, 3 mm and 5 mm are listed in Tables 4–7, respectively. These computations are carried out for various locations (Z_m) of the magnetostrictive layers and listed in Tables 4–7. The vibration suppression time (t_s) versus the distance of magnetostrictive layers from the neutral plane (Z_m) for various thicknesses of magnetostrictive layers (h_m) are plotted in Fig. 5. This includes magnetostrictive layers of thicknesses (h_m) of 1 mm, 2 mm and 3 mm at various locations. From Fig. 5 one can observe that 1 mm thick magnetostrictive layer exhibits better attenuation as compared to 2 mm and 3 mm thick magetostrictive layers.

Therefore, relatively thinner magnetostrictive layer leads to better attenuation characteristics. These results presented here agree qualitatively with the results presented in Pradhan et al. (2001) and He et al. (2002).

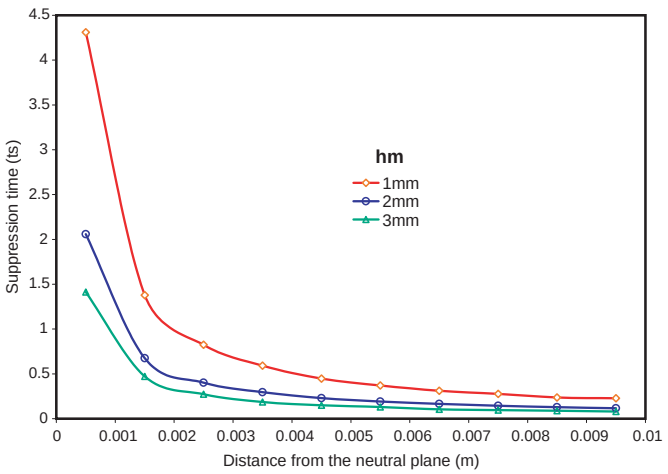

Fig. 5. Vibration suppression time t_s for various thicknesses of magnetostrictive layers (h_m).

4.3. Effect of vibration modes

Effect of higher modes of vibration on the vibration suppression time is studied for the FGM1 shell. Transverse deflection versus time for various cases of the FGM shells are plotted in Figs. 6–8. Fig. 6a–d show the transient response of modes 1, 3, 5 and 7, respectively. It is observed that attenuation favours the higher modes. This is clearly seen in Fig. 7a and b, where modes 1 and 2 are compared for FGM1 and FGM2 shells. These figures indicate that mode 2 attenuates at a significantly faster rate as compared to mode 1. Present results in Fig. 6a–d also show that the vibration suppression time decreases very rapidly as vibration mode number increases. These vibration results for various modes agree qualitatively with the results presented in Pradhan et al. (2001).

4.4. Effect of intensity of control gain

Vibration suppression time (t_s) for the intensity of control gain $C(t)r_c$ values of 1000 and 10,000 are computed and the results are listed in Table 7. This shows that increase of intensity of control gain results in proportional increase in vibration suppression time. From the results listed in Table 7, it is interesting to note that the suppression time ratio (t_s) is directly proportional to the control gain of the applied magnetic field. Further, it is observed that the normalized suppression time ratio (t_n) is independent of the intensity of control gain. These results agree qualitatively with the results presented in Pradhan et al. (2001).

4.5. Effect of material properties of FGM shell

Effect of material properties of the FGM shell on the vibration suppression time is studied. Fig. 8 displays the vibration suppression for FGM1 (Stainless Steel–Nickel) and FGM2 (Nickel–Aluminum

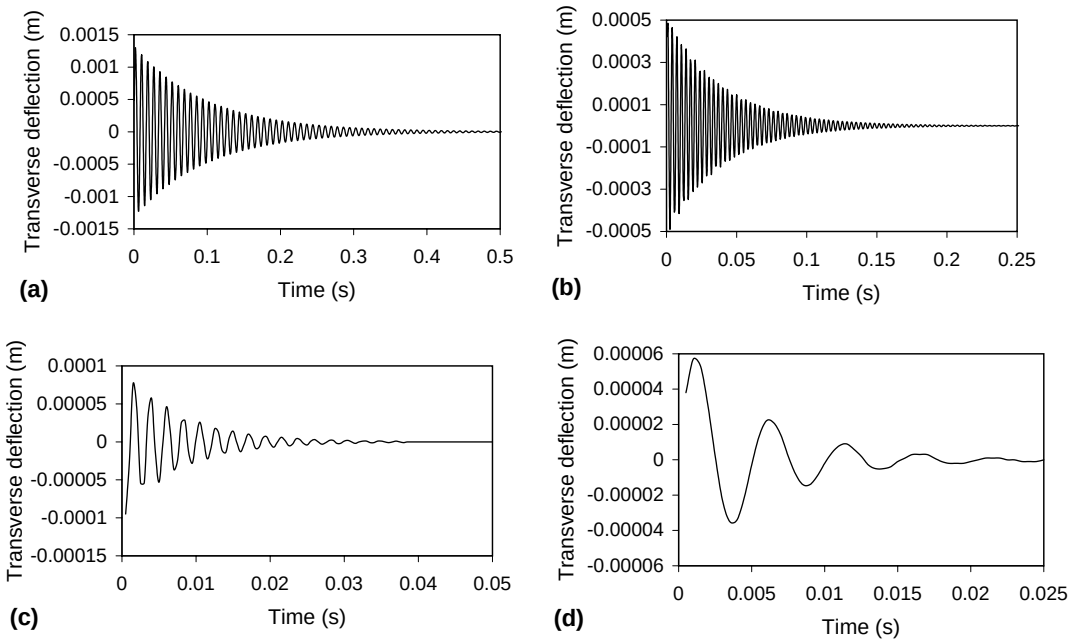

Fig. 6. Vibration suppression of higher modes at the midpoint of the FGM1 shell: (a) $n = 1$, (b) $n = 3$, (c) $n = 5$ and (d) $n = 7$.

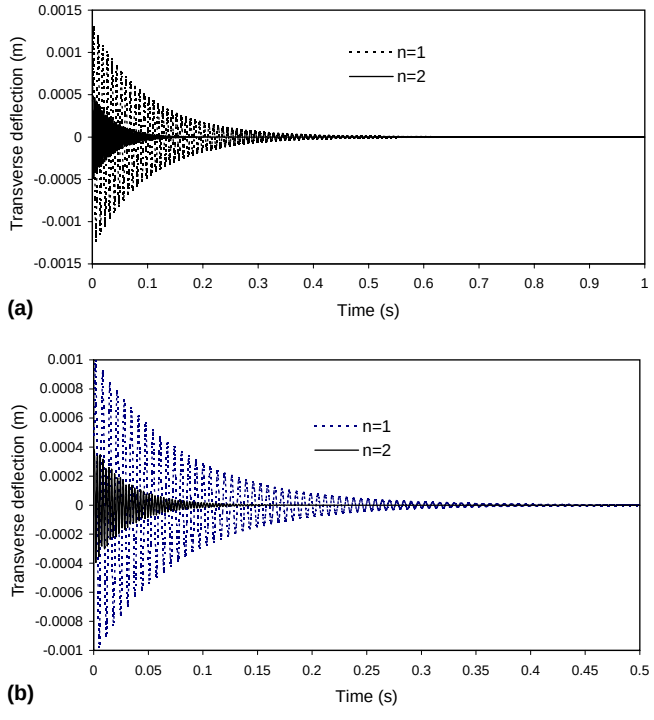

Fig. 7. Comparison of controlled motion at the midpoint of the (a) FGM1 and (b) FGM2 shells for vibration modes $n = 1$ and $n = 2$.

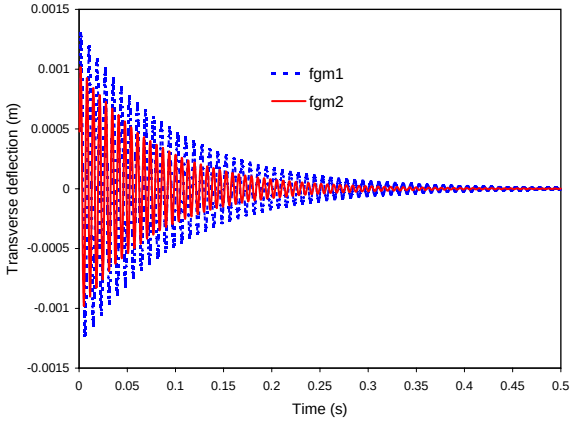

Fig. 8. Vibration suppression of FGM1 and FGM2 shells for $Z_m = 9.5$ mm.

Oxide) shells. For this comparison study Z_m is assumed to be 9.5 mm. From Fig. 8, it is observed that FGM1 shell has lower frequency compared to the FGM2 shell. This confirms that the FGM1 shell has lower flexural rigidity and thus a lower frequency compared to the FGM2 shell. These results agree qualitatively with the results presented in Pradhan et al. (2001).

5. Conclusions

A theoretical formulation for a FGM shell with embedded magnetostrictive layers has been presented. The analytical solutions for the case of simply supported boundary conditions has been derived, and numerical results are presented. The formulation is based on the first-order shear deformation shell theory (FSDT), and the analytical solution for the simply supported shell is based on the Navier solution approach. The effects of the material properties of the FGM shell, thickness of magnetostrictive layers and location of the magnetostrictive layers on the vibration suppression time have been examined in detail. It was found that attenuation effects were better if the magnetostrictive layers were placed farther away from the neutral plane. Attenuation effects were also better when the magnetostrictive layers were relatively thinner. Further, suppression time ratio was directly proportional to the control gain of the applied magnetic field.

Acknowledgement

Author would like to acknowledge the technical discussion and suggestions of Professor J.N. Reddy, Texas A&M University, College Station, USA.

Appendix A

$$S_{11} = A_{11}\alpha^2 + A_{66}\beta^2 + C_0^2 D_{66}\beta^2 + K_S A_{55}\frac{1}{R_1^2} + 2C_0 B_{66}\beta^2$$

$$S_{12} = A_{12}\alpha\beta + A_{66}\alpha\beta - C_0^2 D_{66}\alpha\beta$$

$$S_{13} = -A_{11}\alpha\frac{1}{R_1} - A_{12}\alpha\frac{1}{R_2} - K_S A_{55}\alpha\frac{1}{R_1}$$

$$S_{14} = B_{11}\alpha^2 + B_{66}\beta^2 + C_0\beta^2 D_{66} - K_S A_{55}\frac{1}{R_1}$$

$$S_{15} = B_{12}\alpha\beta + B_{66}\alpha\beta + C_0 D_{66}\alpha\beta$$

$$C_{13} = \mathscr{A}_{31}\alpha, \quad C_{11} = C_{12} = C_{14} = C_{15} = 0$$

$$M_{11} = \left(I_1 + \frac{2I_2}{R_1}\right), \quad M_{14} = \left(I_1 + \frac{I_3}{R_1}\right), \quad M_{12} = M_{13} = M_{15} = 0$$

$$S_{22} = A_{66}\alpha^2 + C_0^2\alpha^2 D_{66} + \beta^2 A_{22} + \frac{A_{44}}{R_2^2} - 2C_0\alpha^2 B_{66}$$

$$S_{23} = -\frac{A_{12}}{R_1}\beta - \frac{A_{22}}{R_2}\beta - K_S\frac{A_{44}}{R_2}\beta$$

$$S_{24} = B_{66}\alpha\beta - C_0 D_{66}\alpha\beta + B_{12}\alpha\beta$$

$$S_{25} = B_{66}\alpha^2 - C_0 D_{66}\alpha^2 + B_{22}\beta^2 - K_S\frac{A_{44}}{R_2}$$

$$C_{23} = \mathscr{A}_{32}\beta, \quad C_{21} = C_{22} = C_{24} = C_{25} = 0$$

$$M_{22} = \left(I_1 + \frac{2I_2}{R_2}\right), \quad M_{25} = \left(I_1 + \frac{I_3}{R_2}\right), \quad M_{21} = M_{23} = M_{24} = 0$$

$$S_{33} = K_S A_{55}\alpha^2 + K_S A_{44}\beta^2 + \frac{A_{11}}{R_1^2} + \frac{2A_{12}}{R_1 R_2} + \frac{A_{22}}{R_2^2}$$

$$S_{34} = -\frac{B_{11}\alpha}{R_1} - \frac{B_{12}\alpha}{R_2} + K_S A_{55}\alpha$$

$$S_{35} = -\frac{B_{12}\beta}{R_1} - \frac{B_{22}\beta}{R_2} + K_S A_{44}\beta$$

$$C_{33} = \frac{\mathscr{A}_{32}}{R_2} + \frac{\mathscr{A}_{31}}{R_1}, \quad C_{31}, C_{32}, C_{34}, C_{35} = 0$$

$$M_{33} = I_1, \quad M_{31}, M_{32} = M_{34} = M_{35} = 0$$

$$S_{44} = D_{11}\alpha^2 + D_{66}\beta^2 + K_S A_{55}$$

$$S_{45} = D_{12}\alpha\beta + D_{66}\alpha\beta$$

$$C_{43} = \mathscr{B}_{31}\alpha, \quad C_{41} = C_{42} = C_{44} = C_{45} = 0$$

$$M_{44} = I_2, \quad M_{41} = M_{14}, \quad M_{42} = M_{43} = M_{45} = 0$$

$$S_{55} = D_{66}\alpha^2 + D_{22}\beta^2 + K_S A_{44}$$

$$C_{53} = \mathscr{B}_{32}\beta, \quad C_{51}, C_{52}, C_{54}, C_{55} = 0$$

$$M_{55} = I_2, \quad M_{52} = M_{25}, \quad M_{51} = M_{53} = M_{54} = 0$$

References

Anjanappa, M., Bi, J., 1994. Magnetostrictive mini actuators for smart structural application. Smart Materials and Structures 3 (4), 383–390.

Baz, A., Imam, K., Mccoy, J., 1990. The dynamics of helical shape memory actuators. Journal of Intelligent Material Systems and Structures 1, 105–133.

Bryant, M.D., Fernandez, B., Wang, N., 1993. Active vibration control in structures using magnetostrictive Terfenol with feedback and/or neural network controllers. Journal of Intelligent Material Systems and Structures 4, 484–489.

Choi, Y., Sprecher, A.F., Conrad, H., 1990. Vibration characteristics of a composite beam containing electrorheological fluid. Journal of Intelligent Material Systems and Structures 1, 91–104.

Crawley, E.F., Luis, J.D., 1987. Use of piezoelectric actuators and elements of intelligent structure. AIAA Journal 25, 1373–1385.

Cross, L.E., Jang, S.J., 1988. Electrostrictive materials. In: Proceedings of Recent Advances in Piezoelectric Ceramics. Electronic Ceramics, Properties, Devices, and Applications. Marcel Dekker, Inc., New York, pp. 129–137.

Friedmann, P.P., Carman, G.P., Millott, T.A., 2001. Magnetostrictively actuated control flaps for vibration reduction in helicopter rotors—Design considerations for implementation. Mathematical and Computer Modelling 33 (10–11), 1203–1217.

Giurgiutiu, V., Jichi, F., Berman, J.B., Kamphaus, J.M., 2001. Theoretical and experimental investigation of magnetostrictive composite beams. Smart Materials and Structures 10 (5), 934–945.

Goodfriend, M.J., Shoop, K.M., 1992. Adaptive characteristics of the magnetostrictive alloy, Terfenol-D, for active vibration control. Journal of Intelligent Material Systems and Structures 3, 245–254.

He, X.Q., Liew, K.M., Ng, T.Y., Sivashanker, S., 2002. A FEM model for the active control of curved FGM shells using piezoelectric sensor/actuator layers. International Journal of Numerical Methods in Engineering 54 (6), 853–870.

Krishna Murty, A.V., Anjanappa, M., Wu, Y.-F., 1997. The use of magnetostrictive particle actuators for vibration attenuation of flexible beams. Journal of Sound and Vibration 206 (2), 133–149.

Loy, C.T., Lam, K.Y., Reddy, J.N., 1999. Vibration of functionally graded cylindrical shells. International Journal of Mechanical Science 41 (3), 309–324.

Pradhan, S.C., Loy, C.T., Lam, K.Y., Reddy, J.N., 2000. Vibration characteristics of functionally graded cylindrical shells under various boundary conditions. Applied Acoustics 61 (1), 111–129.

Pradhan, S.C., Ng, T.Y., Lam, K.Y., Reddy, J.N., 2001. Control of laminated composite plates using magnetostrictive layers. Smart Materials and Structures 10 (4), 657–667.

Reddy, J.N., 1984a. Energy and Variational Methods in Applied Mechanics: With an Introduction to the Finite Element Method. Wiley, New York.

Reddy, J.N., 1984b. Exact solutions of moderately thick laminated shells. Journal of Engineering Mechanics ASCE 110 (5), 794–809.

Uchino, K., 1986. Electrostrictive actuators: Materials and applications. Ceramics Bulletin 65, 647–652.

Woo, J., Meguid, S.A., 2001. Nonlinear analysis of functionally graded plates and shallow shells. International Journal of Solids and Structures 38 (42–43), 7409–7421.